Electronic Supplementary Information

Efficient Ammonia Synthesis *via* Electroreduction of Nitrite Using Single-atom Ru-Doped Cu Nanowire Arrays

Ngoc Quang Tran,[ab*] Le Thai Duy,[c] Dai Cao Truong,[ab] Bao Thu Nguyen Le,[bd] Bach Thang Phan,[ab] Yunhee Cho,[ef] Xinghui Liu,[e] Hyoyoung Lee[efg*]

[a] *Center for Innovative Materials and Architectures, Ho Chi Minh City, Viet Nam*

[b] *Vietnam National University, Ho Chi Minh City, Viet Nam*

[c] *Department of Materials Science and Engineering, Ajou University, Suwon 16499, Korea*

[d] *Department of Mathematics and Physics, University of Information Technology, Ho Chi Minh City, Viet Nam*

[e] *Center for Integrated Nanostructure Physics, Institute for Basic Science (IBS), Sungkyunkwan University, Suwon 16419, Republic of Korea.*

[f] *Department of Chemistry, Sungkyunkwan University, Suwon 16419, Republic of Korea.*

[g] *Department of Biophysics, Sungkyunkwan University, Suwon 16419, Republic of Korea.*

**To whom correspondence should be addressed. Email: tnquang@inomar.edu.vn, hyoyoung@skku.edu*

Preparation of Ru-Cu NW/CF. $Cu(OH)_2$ NW array was grown on a copper foam (CF) by a simple chemical oxidation method. Firstly, the CF was cleaned ultrasonically in a dilute HCl solution, ethanol, and deionized water three times. The obtained CF was immersed into 30 mL of an aqueous solution containing 0.05 mol L^{-1} $(NH_4)_2S_2O_8$ and 1 mol L^{-1} NaOH at room temperature for 20 min. Afterward, the light blue color product was washed several times with ethanol/water and dried in a vacuum oven overnight. Then, the as-prepared $Cu(OH)_2$ NW/CF was immersed into 5 mL of an aqueous solution containing 5 mmol L^{-1} of $RuCl_3$ for 2 h at room temperature to obtain Ru-$Cu(OH)_2$ NW/CF. After washing several times with deionized water, the Ru-$Cu(OH)_2$ NW/CF was thermally annealed at 180 °C for 1 h under air. Finally, the Ru-$Cu(OH)_2$ NW/CF was electrochemically reduced at -1.08 V vs. Ag/AgCl in an Ar-saturated 1 M $NaHCO_3$ solution to obtain Ru-Cu NW/CF.

Physicochemical characterization. Powder X-ray diffraction (XRD) measurements were performed at room temperature with Cu kα1 radiation by means of a Rigaku Ultima IV. The surface morphology and structure of the catalysts were investigated by transmission electron microscopy (TEM, JEOL JEM-2100F) and field emission scanning electron microscopy (FESEM, FEI Quanta FEG 400). X-ray photoemission spectroscopy (XPS, ESCA 2000, VG Microtech) measurements with an aluminum anode (Al Kα = 1,486.6 eV) were carried out at 150 W for the surface chemical state and elemental compositions analysis. All of the XPS spectra were calibrated with the C 1s peak (set as 284.4 eV). The atomic percentages of Ru single atoms were determined using inductively coupled plasma mass spectrometry (ICP-MS, Agilent 7500ce ICP-MS).

Ru K-edge X-ray absorption measurement. X-ray absorption measurements at the Ru K-edge were performed at the 1W1B station in the Beijing Synchrotron Radiation Facility (BSRF). The storage rings of BSRF were conducted at 2.5 GeV with an average current of 250 mA. By using a

Si (111) double-crystal monochromator, the data collection was carried out in the transmission/fluorescence mode using an ionization chamber. All spectra were collected under ambient conditions.

Electrochemical NO_2 reduction reaction measurements. All electrochemical measurements were performed using a three-electrode gas-tight two-compartment electrochemical cell at ambient conditions using a VMP3 electrochemical workstation (Biologic Science Instruments, France). The obtained Ru-Cu NW/CF (1 cm x 1 cm) was directly used as a working electrode. The SCE reference electrode and working electrode were placed in the cathodic compartment. The Pt foil counter electrode was placed in the anodic compartment, separated by a Nafion membrane. Prior to the test, the Nafion 117 membrane was pretreated by successive immersion in a 5% H_2O_2 solution at 80 ºC for 1 h and deionized water for another 1 h at 80 ºC. 45 mL of 0.1 M PBS (pH=7) that contained 500 ppm of NO_2^- ($NaNO_2$) was used as the electrolyte. All potentials were converted to the RHE scale based on the Nernst equation. Controlled potential electrolysis was conducted at different applied potentials for 1 h.

Determination of the produced ammonia. The quantitative ammonia concentration in the as-produced 0.1 M PBS electrolyte was determined using the indophenol blue method. Due to the high concentrations of products, the obtained electrolytes were diluted by a factor of ten. Typically, 2 mL of obtained electrolyte was added into a 1 M NaOH solution (2 mL) containing 5 wt% salicylic acid and 5 wt% sodium citrate. Then, 1 mL of 0.05 M NaClO and 0.2 mL of 1 wt% $C_5FeN_6Na_2O$ were successively added into the above solution. After 1 h at room temperature, the mixed solutions were evaluated using a UV-vis absorption spectrophotometer. The concentration of indophenol blue was determined based on the absorbance peak at a wavelength of 655 nm. To obtain the concentration-absorbance calibration curves, we measured a series of concentrations of

standard NH_4^+ in 0.1 M PBS solutions.

Determination of the produced hydrazine. The amount of hydrazine in the electrolyte was determined by the Watt and Chrisp method. The composition of the chromogenic reagent was first prepared by mixing 1.497 g of para-(dimethylamino) benzaldehyde, 7.5 mL of concentrated HCl, and 75 mL of ethanol. Then, 5 mL of the obtained electrolyte was added into 5 mL of the above solution. The absorbance of the resulting solution was measured at a wavelength of 460 nm. To estimate the concentration-absorbance calibration curves, a series of concentrations of standard hydrazine in 0.1 M PBS solutions were prepared.

1H NMR experiment. After electrolysis for one hour at -0.6 V *vs.* RHE in 0.1 M PBS that contained 500 ppm of NO_2^- as the electrolyte, 0.2 mL of the resulting solution was removed. Then, 8 μL of D_2O, which contains 1 w/w% of 3-(trimethylsilyl)-1-propanesulfonic acid sodium salt as an internal standard, was added to 0.2 mL of the above electrolyte. The obtained amount of $^{15}NH_4$ was quantitatively determined by 1H NMR spectroscopy.

The calculation method for the Faraday efficiency and yield rate

The Faraday efficiency (FE) and yield rate of the NH_3 product were calculated as follows.

$$FE = \frac{[N * F * c(NH_3) * V]}{Q}$$

$$Yield\ rate_{mass}(NH_3) = \frac{[17c(NH_3) * V]}{t * A}$$

N = 6: the number of electrons transferred for NH_3 product formation

F = 96,485 C/mol: Faraday constant

$c(NH_3)$: measured NH_3 concentration

V = 45 mL: volume of the 0.1 M PBS electrolyte

Q: total charge passed through the working electrode

t = 1 h: electrolysis time

A = 1 cm^2: the area of the working electrode

Calculation method

The present first principle DFT calculations are performed by Vienna Ab initio Simulation Package (VASP)[1] with the projector augmented wave (PAW) method.[2] The exchange-functional was treated using the generalized gradient approximation (GGA) of Perdew-Burke-Ernzerhof (PBE) functional.[3] The energy cutoff for the plane-wave basis expansion was set to 450 eV, and the force on each atom was set to less than 0.03 eV/Å for the convergence criterion of geometry relaxation. The Brillouin zone was sampled with 3 × 3 × 1 Monkhorst mesh. The self-consistent calculations were done by applying a convergence energy threshold of 10^{-5} eV. The DFT-D3 method was employed to consider the van der Waals interaction.[4] A 15 Å vacuum was added along the z-direction in order to avoid the interaction between periodic structures.

The free energies of the NO_2 reduction steps were calculated by the equation:[5] $\Delta G = \Delta E_{DFT} + \Delta E_{ZPE} - T\Delta S$, where ΔE_{DFT} is the DFT electronic energy difference of each step, ΔE_{ZPE} and ΔS are the correction of zero-point energy and the variation of entropy, respectively, which are obtained by vibration analysis, and T is the temperature (T = 300 K).

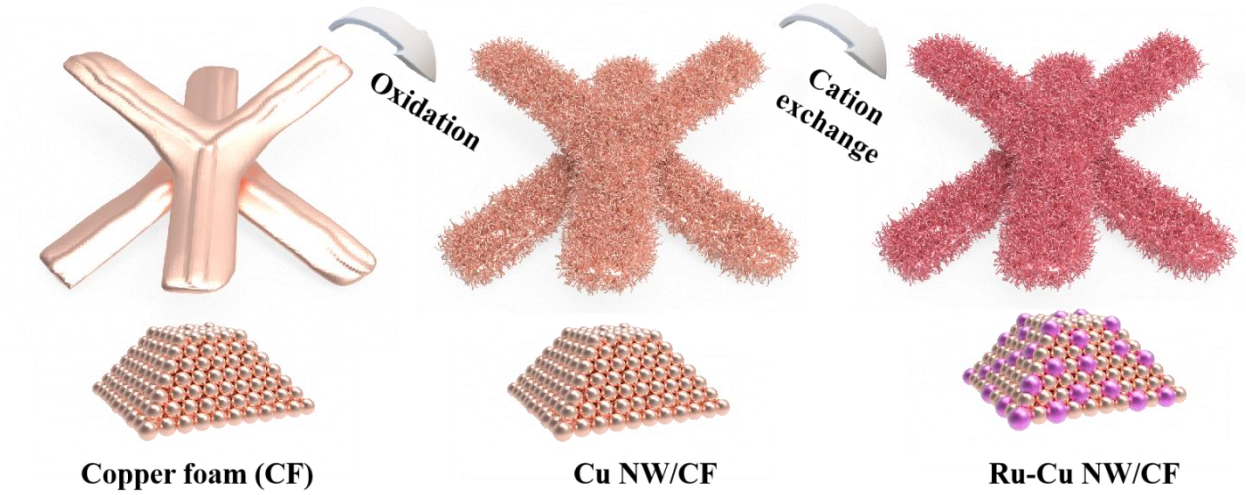

Fig. S1 Schematic illustration of the synthesis pathway for Ru-Cu NW/CF.

Our strategy to synthesize Ru Cu NW/CF is illustrated in Fig. S1. We firstly prepared $Cu(OH)_2$ NWs on copper foam (CF) by a simple chemical oxidation method. Then, the obtained $Cu(OH)_2$ NW/CF was immersed into an aqueous solution containing $RuCl_3$ for 2 h at room temperature to obtain Ru $Cu(OH)_2$ NW/CF. Finally, the Ru $Cu(OH)_2$ NW/CF was electrochemically reduced to o btain Ru-Cu NW/CF.

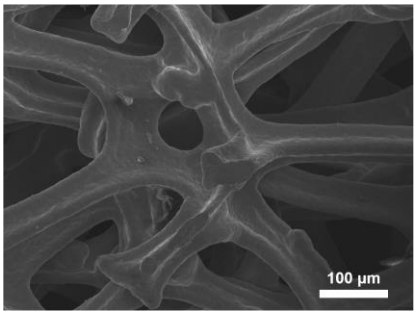

Fig. S2 FESEM images of the bare Copper foam (CF).

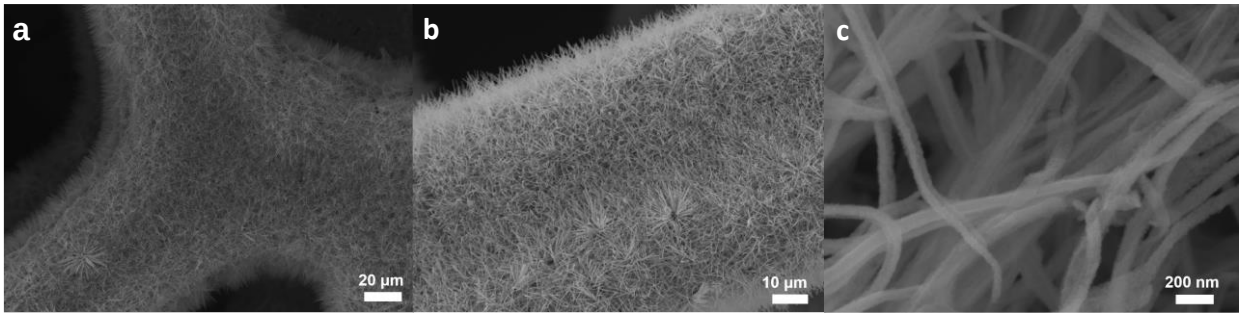

Fig. S3 (a-c) FESEM images of the Cu NW/CF with different magnifications.

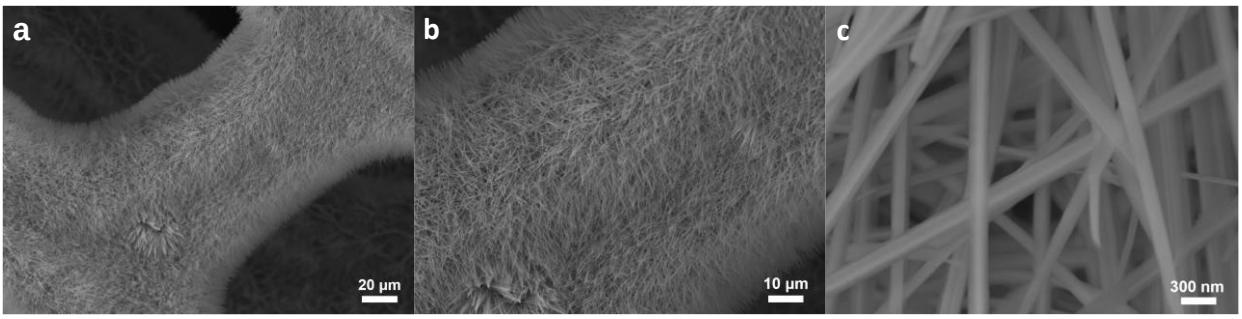

Fig. S4 (a-c) FESEM elemental mapping images of $Cu(OH)_2$ NW/CF with different magnifications.

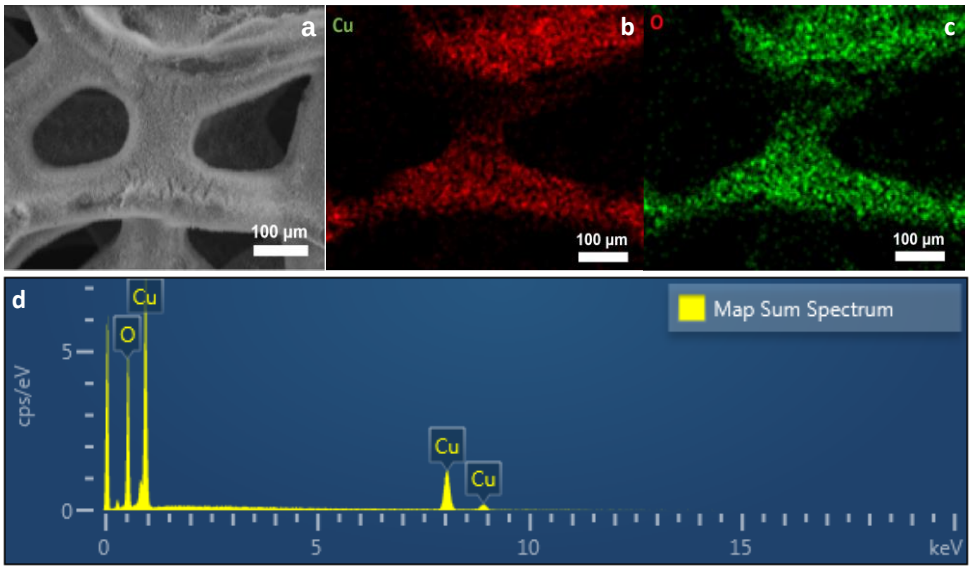

Fig. S5 (a-c) FESEM images of the $Cu(OH)_2$ NW/CF. (d) EDX pattern of $Cu(OH)_2$ NW/CF.

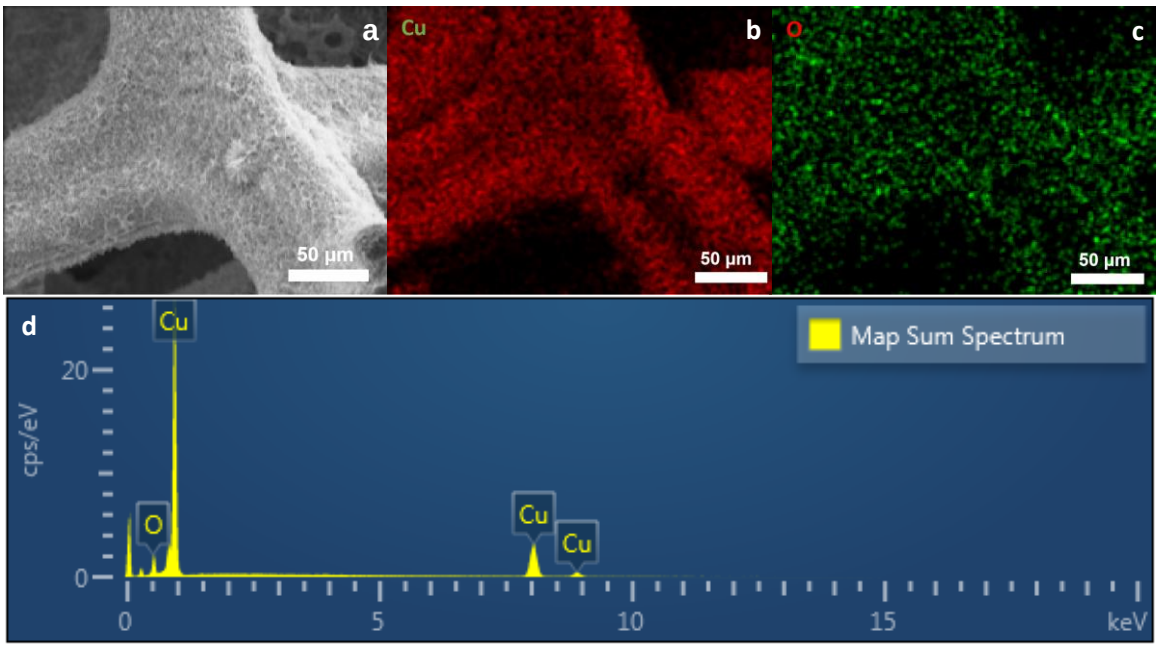

Fig. S6 (a-c) FESEM images of the Cu NW/CF. (d) EDX pattern of Cu NW/CF.

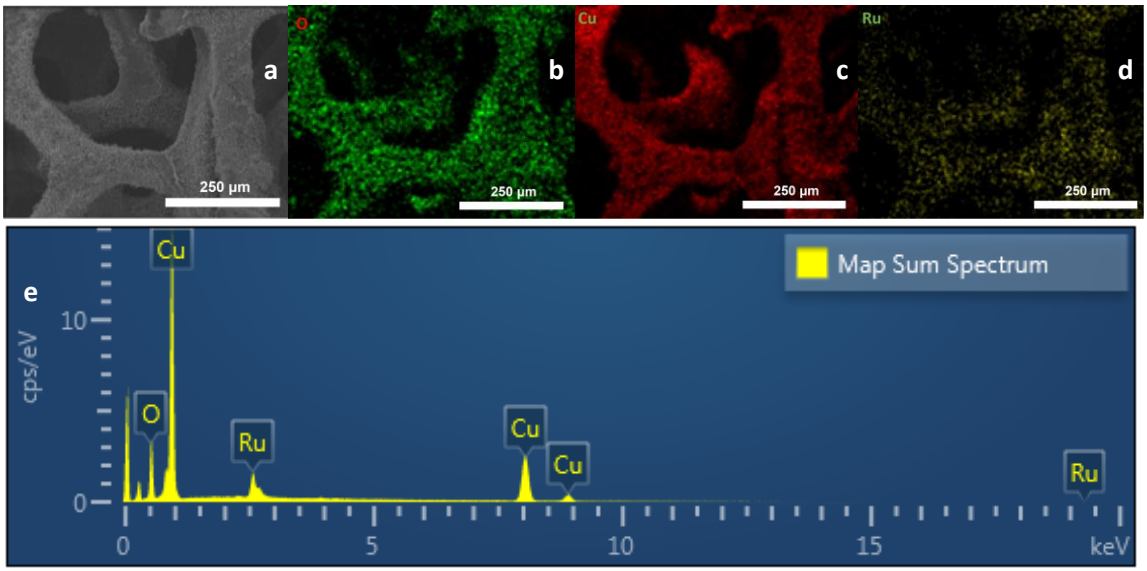

Fig. S7 (a-d) FESEM elemental mapping images of Ru-Cu NW/CF, (e) EDX pattern of Ru-Cu NW/CF.

Supplementary Table S1: EDX analysis of Ru-Cu NW/CF sample

Element	Line Type	wt%	wt% sigma	Atomic%
O	K series	10.90	0.46	31.18

Cu	K series	81.75	0.64	64.37
Ru	L series	7.35	0.60	4.45
Total:		100		100

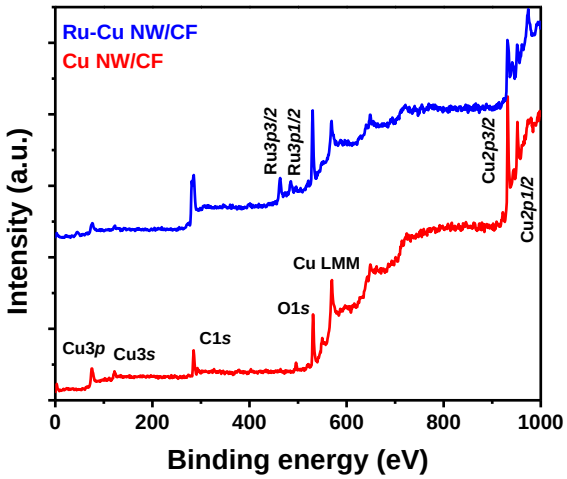

Fig. S8 The survey XPS spectra of Cu NW/CF and Ru-Cu NW/CF.

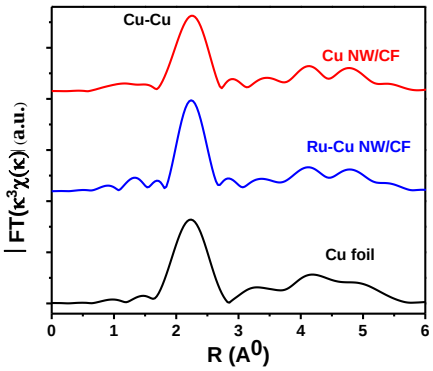

Fig. S9 Fourier transform of Cu K-edge EXAFS spectra.

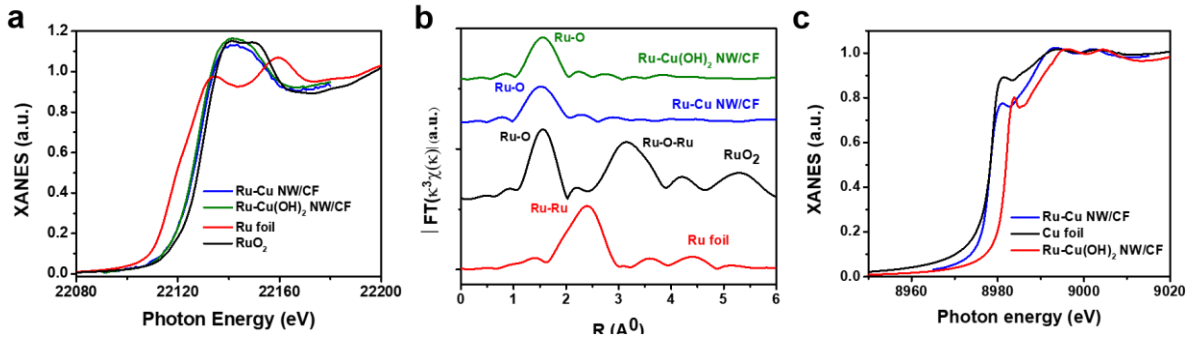

Fig. S10 (a) Ru K-edge XANES spectra, (b) Fourier transform of Ru K-edge EXAFS spectra, and (c) Cu K-edge XANES spectra of Ru-$Cu(OH)_2$ NW/CF.

The Ru K-edge XANES and Fourier transform of Ru K-edge EXAFS spectra of Ru-$Cu(OH)_2$ NW/CF sample are very similar to those of the Ru-Cu NW/CF, suggesting that well-defined Ru single atoms were atomically dispersed in the $Cu(OH)_2$ NW. As shown in Supplementary Fig. S10, the absorption edge of Ru-$Cu(OH)_2$ NW/CF show a distinct shift towards high energies as the valence of Cu ions increase.

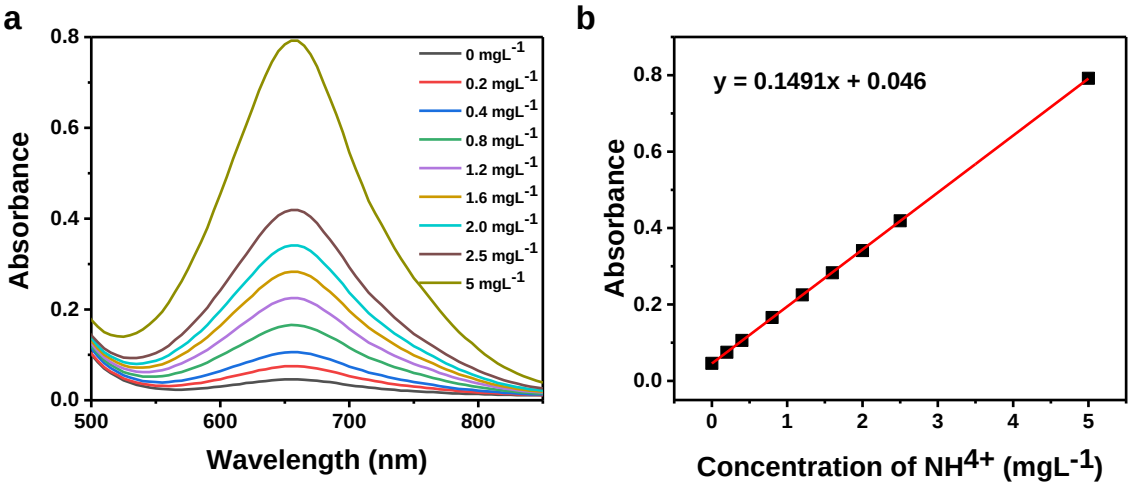

Fig. S11 (a) UV-Vis curves of indophenol blue method, (b) Concentration-absorbance curve of NH_4^+ ions solutions with a species of standard concentration.

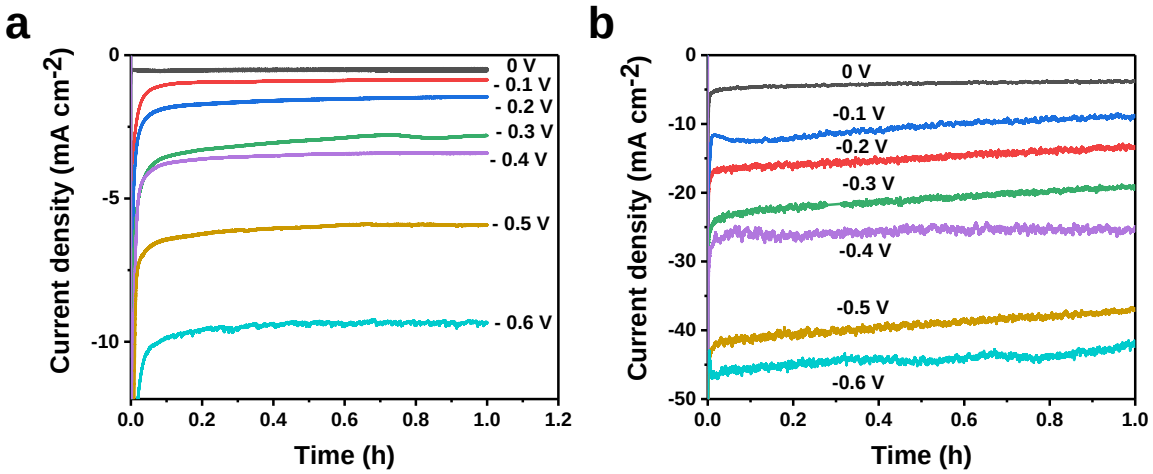

Fig. S12 Chronoamperometry results of (a) Cu NW/CF and (b) Ru-Cu NW/CF recorded at various applied potentials for 1 h.

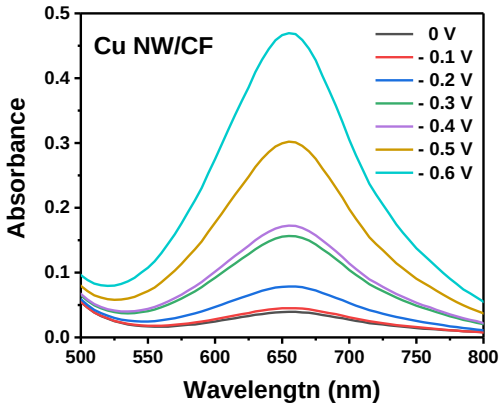

Fig. S13 UV-vis spectroscopy of the electrolytes stained with an indophenol indicator of Cu NW/CF.

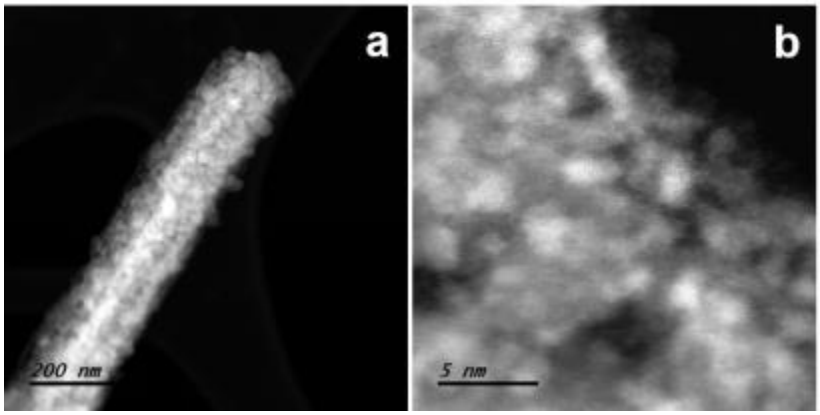

Fig. S14 HADDF-STEM images of Ru NP-Cu NW/CF at low (a) and high (b) magnification.

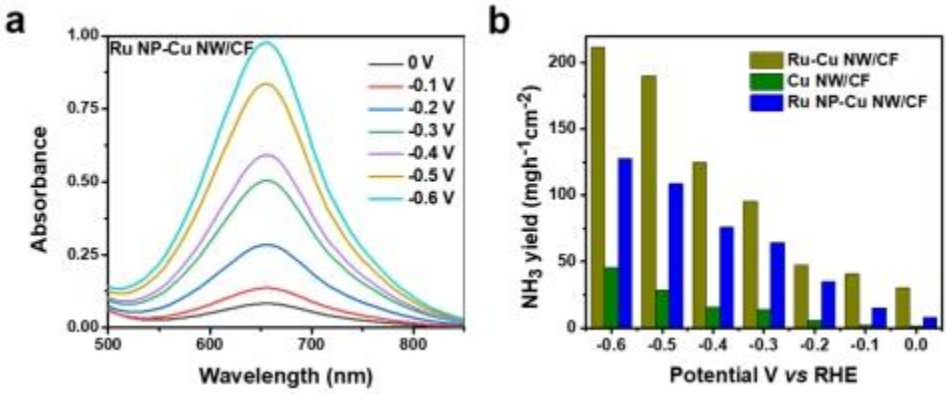

Fig. S 15 (a) UV-vis spectroscopy results of the electrolytes stained with an indophenol indicator of Ru NP-Cu NW/CF. (b) NH_3 yield rate of Cu NW/CF, Ru-Cu NW/CF and Ru NP-Cu NW/CF at different applied potentials.

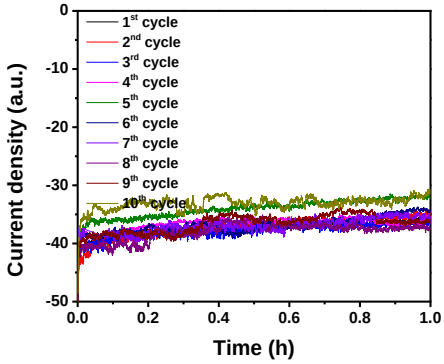

Fig. S16 Chronoamperometry results of Ru-Cu NW/CF.

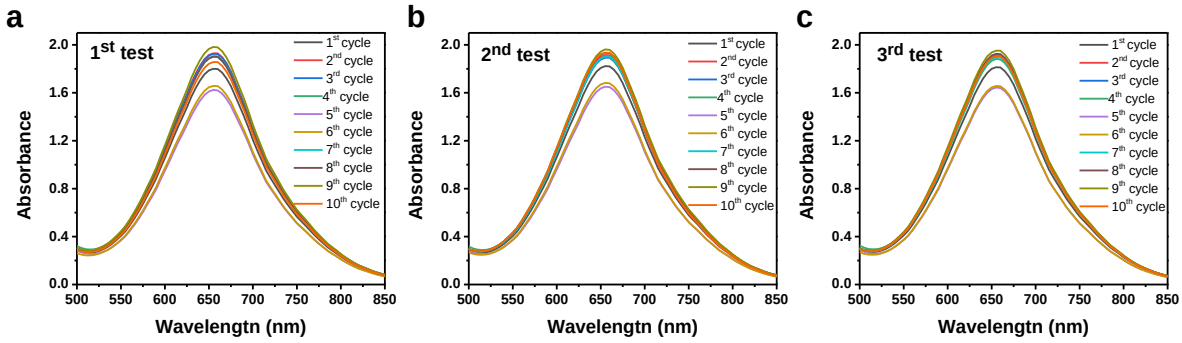

Fig. S17 (a-c) UV-vis spectroscopy of the electrolytes stained with an indophenol indicator at different cycling stability tests of Ru-Cu NW/CF at -0.5 V *vs* RHE.

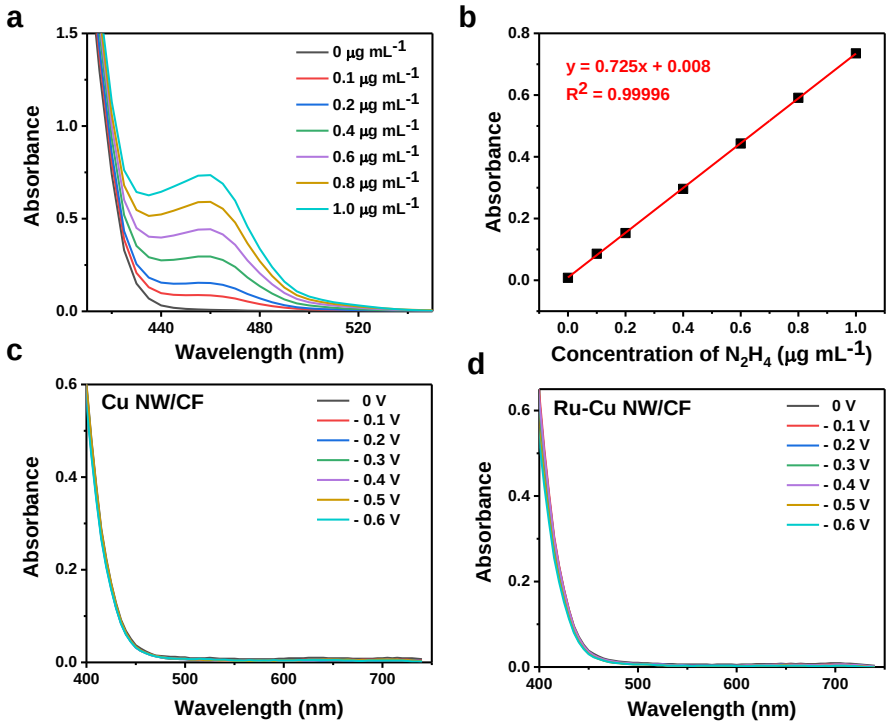

Fig. S18 (a) UV-vis spectroscopy of various $N_2H_4.H_2O$ standard concentrations, (b) calibration curve used for the estimation of the $N_2H_4.H_2O$ standard concentration, UV-vis spectroscopy of the electrolytes for Cu NW/CF (c) and Ru-Cu NW/CF (d).

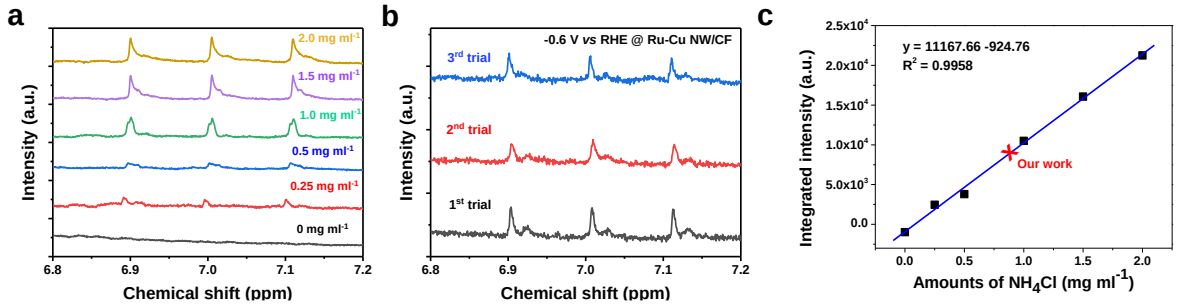

Figure. S19 (a) ^{1}H NMR spectra of the standard solutions with various NH_4Cl concentrations, (b) ^{1}H NMR spectra of the NH_4^+ yielded by the Ru-Cu NW/CF electrode, and (c) the corresponding NH_4^+ calibration curve constructed by plotting the integrated peak areas.

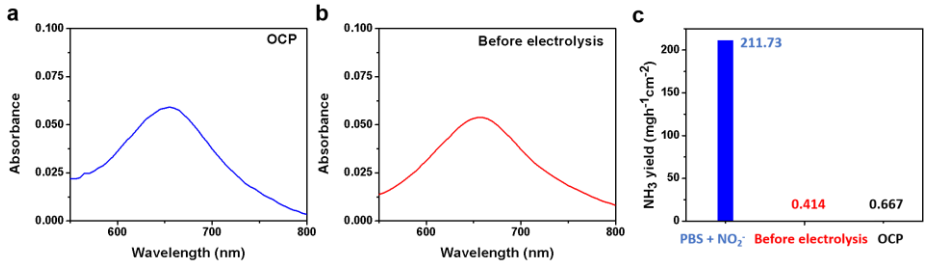

Fig. S20 UV-vis spectroscopy results of the electrolytes stained with an indophenol indicator of Ru-Cu NW/CF under (a) OCP and (b) before electrolysis. (c) Amounts of produced NH_3 under different conditions.

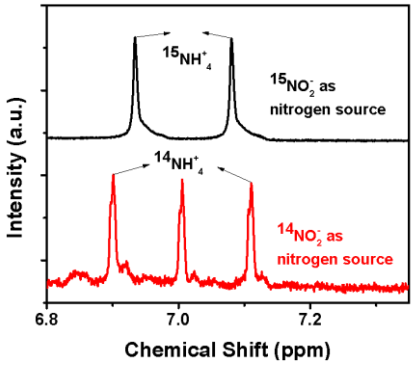

Fig. S21 ^{1}H NMR spectra of Ru-Cu NW/CF catalyst after electrochemical reduction using $^{15}NO_2^-$ and $^{14}NO^-_2$.

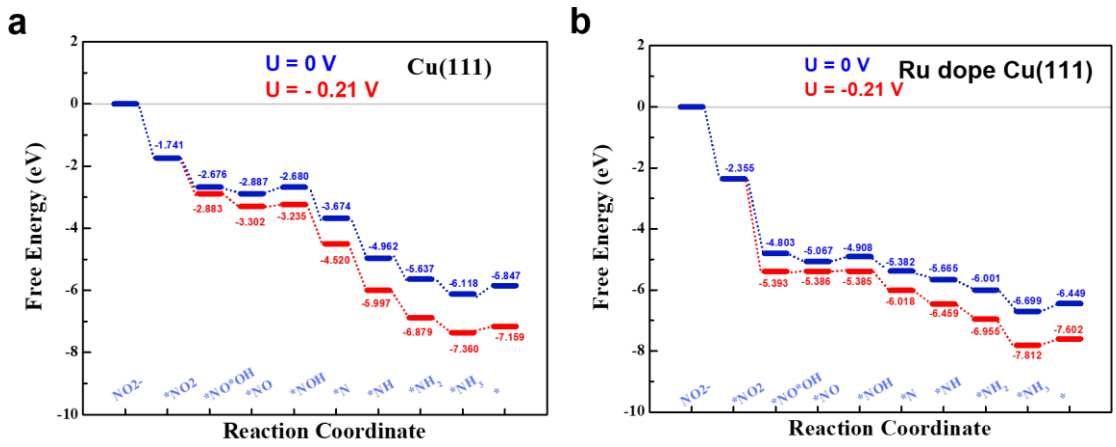

Fig. S22 Free energy diagram of different intermediates generated during electrocatalytic NO_2^- reduction at the different applied potential on the (a) Cu(111) and (b) Ru-doped Cu(111).

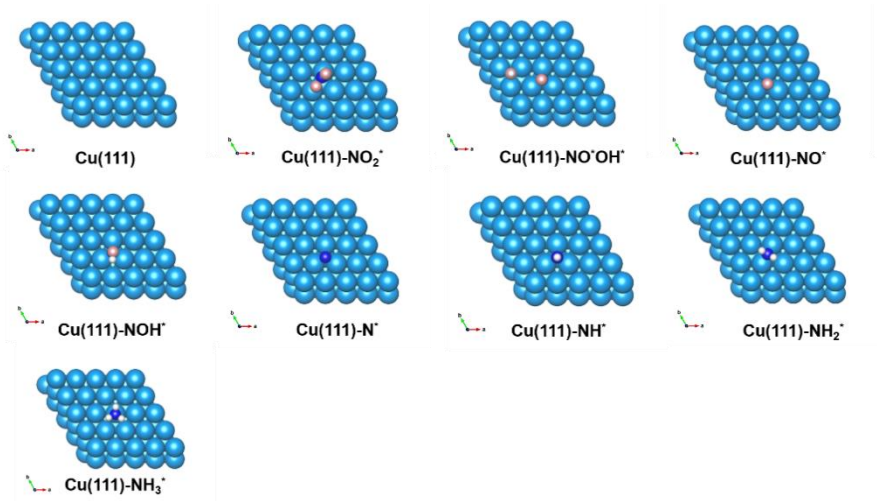

Fig. 23 The corresponding optimized atomic configurations of the adsorbed intermediates on Cu(111).

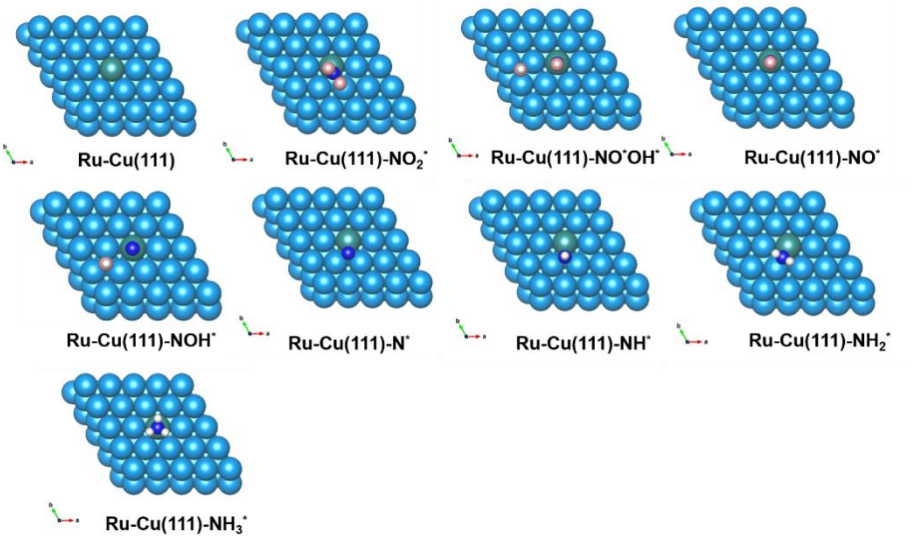

Fig. 24 The corresponding optimized atomic configurations of the adsorbed intermediates on Ru-doped Cu(111).

Supplementary Table S2: Ammonia yield rate and Faraday efficiency of our catalyst compared with other reported catalysts.

Catalyst	Electrolyte	NH_3 yield rate	Faraday efficiency (%)	Ref.
CF@Cu_2O	0.1 M PBS (0.1 M $NaNO_2$)	7510.73 μg h^{-1} cm^{-2}	94.21 %	*Chem. Commun., 2022, 58, 517–520.*
TiO_{2-x} NBA/TP	0.1 M NaOH ($NaNO_2$)	7898 μg h^{-1} cm^{-2}	92.7 %	***Chem. Commun.***, 2022, Accepted https://doi.org/10.1039/D2CC00856D
Cu_3P NA/CF	0.1 M PBS (0.1 M $NaNO_2$)	1626.6 ±36.1 μg h^{-1} cm^{-2}	91.2 ±2.3 %	*Green Chem.*, 2021, **23**, 5487–5493.
CoP nanoarray	0.1 M PBS (500 ppm $NaNO_2$)	2260.7 ± 51.5 μg h^{-1} cm^{-2}	90 ± 2.3 %	*Nano Res., 2022, 15, 972–977.*
Ni_2P nanosheet array	0.1 M PBS	2692.2 ± 92.1 μg h^{-1} cm^{-2}	90.2 ± 3 %	*J. Colloid Interface Sci., 2022, 606, 1055–1063.*

	(200 ppm $NaNO_2$)			
Ni-NSA-V_{Ni}	0.2 M Na_2SO_4 (200 ppm $NaNO_2$)	235.98 μmol h^{-1} cm^{-2}	88.9 %	*J. Mater. Chem. A, 2021, 9, 239–243.*
MnO_2 nanoarrays	0.1 M Na_2SO_4 ($NaNO_2$)	3.09 x 10^{-11} mol s^{-1} cm^{-2}	6 %	*Chem. Commun., 2018, 54, 10340–10342.*
Cobalt-tripeptide complex	0.1 M MOPS (1M $NaNO_2$)	3.01 x 10^{-10} mol s^{-1} cm^{-2}	90 ± 3 %	*J. Am. Chem. Soc., 2018, 140, 16888–16892.*
MoFe protein	0.25 M HEPES buffer (0.05 M $NaNO_2$)	0.468 μmol h^{-1} cm^{-2}	100 %	*Energy Environ. Sci., 2016, 9, 2550–2554.*
Cobalt (II) porphyrazine	0.5 M NaOH (0.0028 M $NaNO_2$)	37.1 μmol h^{-1} cm^{-2}	97.0 %	*J. Electroanal. Chem., 1999, 27, 126-135*
Ru-Cu NW/CF	0.1 M PBS (500 ppm $NaNO_2$)	211.73 mg h^{-1} cm-2 732 μmol h^{-1} cm^{-2}	94.1 %	*This work*

References

1 Kresse, G.; Furthmüller, *J. Comp Mater Sci* 1996, **6**, (1), 15-50.

2 Blöchl, P. E. *Phys. Rev. B* 1994, **50**, (24), 17953-17979.

3 Perdew, J. P.; Chevary, J. A.; Vosko, S. H.; Jackson, K. A.; Pederson, M. R.; Singh, D. J.; Fiolhais, C. *Phys. Rev. B* 1992, **46**, (11), 6671-6687.

4 S. Grimme, J. Antony, S. Ehrlich, H. Krieg, *J. Chem. Phys*. 2010, **132**, 154104.

5 Skulason, E.; Bligaard, T.; Gudmundsdottir, S.; Studt, F.; Rossmeisl, J.; Abild-Pedersen, F.; Vegge, T.; Jonsson, H.; Norskov, J. K. *Phys. Chem. Chem. Phys*. 2012, **14**, 1235.